Influence of oxidation on fatigue crack initiation and propagation in turbine disc alloy N18

Jiang, R.; Everitt, S.; Gao, N.; Soady, K.; Brooks, Jeffery; Reed, P.a.s.

DOI:
10.1016/j.ijfatigue.2015.02.007

Influence of oxidation on fatigue crack initiation and propagation in turbine disc alloy N18

R. Jiang, S. Everitt, N. Gao, K. Soady, J.W. Brooks, P.A.S. Reed

PII: S0142-1123(15)00044-4
DOI: http://dx.doi.org/10.1016/j.ijfatigue.2015.02.007
Reference: JIJF 3520

To appear in: *International Journal of Fatigue*

Received Date: 15 October 2014
Revised Date: 6 February 2015
Accepted Date: 13 February 2015

Please cite this article as: Jiang, R., Everitt, S., Gao, N., Soady, K., Brooks, J.W., Reed, P.A.S., Influence of oxidation on fatigue crack initiation and propagation in turbine disc alloy N18, *International Journal of Fatigue* (2015), doi: http://dx.doi.org/10.1016/j.ijfatigue.2015.02.007

Influence of oxidation on fatigue crack initiation and propagation in turbine disc alloy N18

R. Jiang[1*], S. Everitt[1,2], N. Gao[1], K. Soady[1], J.W. Brooks[3] and P. A. S. Reed[1]

[1]Materials Research Group, Engineering and the Environment, University of Southampton, Highfield, Southampton, Hampshire SO17 1BJ, UK

[2]QinetiQ, Boscombe Down, Salisbury, Wiltshire SP4 0JF, UK

[3]University of Birmingham, Edgbaston, Birmingham, West Midlands B15 2TT, UK

*Corresponding author. Tel: +44 (0)23 80599450; Fax: +44 (0)23 80593016;

Email: Rong.Jiang@soton.ac.uk

Abstract:

Fatigue crack initiation and propagation behaviour in subsolvus heat treated turbine disc alloy N18 has been assessed in air and vacuum at 650 and 725^{o}C under three-point loading. Fatigue crack initiation processes have been evaluated using single edge U-notch specimens under a 1-1-1-1 trapezoidal loading waveform along with interrupted tests at 650^{o}C to allow intermittent observations of the notch surface. The results show apparent grain boundary (GB) oxidation can occur under an oxygen partial pressure of 10^{-2}~10^{-3}Pa. Cracks mainly initiate from grain boundaries or γ/γ′ interfaces due to the formation and subsequent cracking of Cr-rich and/or Co-rich oxides, and occasionally initiate from surface pores. Fatigue life in these tests appears to be dominated by this crack initiation process and is significantly reduced by increasing temperature and/or application of an oxidizing environment. Crack growth tests conducted under 1-1-1-1 and 1-20-1-1 loading waveforms indicate that oxidation significantly degrades the crack growth resistance of N18 and is associated with more intergranular fracture surface features. Additional oxidation effects on propagation caused by higher temperature or prolonging dwell time appear limited, whereas a prolonged dwell period seems to instead promote additional creep process, which further enhance crack growth, especially at higher temperature.

Keywords: Ni-based superalloy; stress assisted oxidation; fatigue crack; creep; apparent activation energy

1. Introduction

Aeroengine turbine discs operate at elevated temperatures under dynamic loads in an aggressive service environment over significant periods of time, this requires disc materials to possess high strength at elevated temperatures, good fatigue and creep performance under these service conditions, along with excellent oxidation and corrosion resistance. Powder metallurgy (PM) Ni-based superalloys have been widely used for aeroengine turbine disc application due to their exceptional combined mechanical properties at elevated temperatures in combination with good oxidation/corrosion resistance [1-3]. However, oxidation accelerated fatigue failure (shorter fatigue life or faster crack growth rate) is usually observed when assessing the fatigue performance of disc alloys at elevated temperatures, especially when a dwell period is applied at the peak load [4-10]. Such a phenomenon is usually associated with intergranular fracture resulting from the interaction between GB oxidation/embrittlement effects and mechanical fatigue processes [8, 11-16]. The varying extent of intergranular fracture features observed is the consequence of the competitive effects of oxidation and cyclic fatigue processes in the advancing crack. Generally, intergranular features are dominant on the fracture surface when oxidation makes a significant contribution to the crack tip failure process, whereas transgranular fracture features dominate when the effect of oxidation is absent or is weak [4, 17, 18]. In some cases, a transition from intergranular features to transgranular features can be observed on the fracture surface as the stress intensity factor range (ΔK) increases, indicating the point where the mechanically-driven crack propagation process outstrips the crack tip oxidation process [18].

Extensive studies have shown that the poorer fatigue performance of disc alloys in an oxidizing environment is closely related to oxidation enhanced crack initiation and/or propagation which are associated with stress assisted oxygen diffusion and resultant oxidation [6, 10, 11, 16, 19]. It is generally considered that enhanced crack initiation is mainly caused by GB oxide cracking due to the brittle nature of the formed oxides. The additional stress concentration arising from volume expansion/contraction because of the formation of these oxides may facilitate the cracking process [19]. In addition, the reduced GB sliding and migration ability caused by the absorption of oxygen or other embrittlement agents (released by chemical reactions because of the involvement of oxygen) may lead to the build-up of local stress at these regions, which further results in crack initiation [20]. The enhanced crack propagation associated with intergranular fracture is usually ascribed to

decohesion/reduction in cohesion strength of GBs ahead of the crack tip due to dynamic embrittlement [14, 15] or GB oxide/matrix-oxide interface cracking caused by stress assisted grain boundary oxidation (SAGBO) [8, 11-13].

The oxidation accelerated fatigue failure caused by stress assisted oxygen diffusion and oxidation along grain boundaries is a complex process. It is reported that this process is mainly dependent on oxygen partial pressure, temperature and local stress/strain level, as well as composition and microstructure of investigated alloys [5, 6, 18, 21-23]. For instance, a transitional oxygen partial pressure that is independent of loading conditions but is sensitive to Cr content is observed in fatigue crack growth data of disc alloy Inconel 718 [6]. Above this transitional pressure, a significantly accelerated crack growth occurs, which is believed to be caused by the formation of Ni oxide rather than the dense Cr_2O_3 ahead of the crack tip. Additionally, considerable research on disc alloys, such as U720Li [5] and LSHR alloy [18], has shown that higher temperature and longer dwell at the peak load (which are associated with higher diffusivity and longer diffusion time respectively) are inclined to promote crack growth due to the synergistic oxidation-fatigue effect in an oxidizing environment. This effect is much more significant in the fine grained variants of these disc alloys which are able to provide more grain boundaries acting as short-circuit diffusion paths [5, 18, 23]. It is relatively complex to quantitatively evaluate unambiguously the simple effect of alloy composition on crack growth. This is due to the varying microstructure, grain boundary character and mechanical properties caused by not only the varying composition, but differing mechanical processing and heat treatment approaches, although some efforts have been made [4, 22, 24].

N18 is a PM disc superalloy, developed for the SNECMA M88 engine used in the RAFALE aircraft [1]. It is designed for long-term use at 650^{o}C and limited use at 700^{o}C. A trade-off between good fatigue crack growth and oxidation resistance as well as excellent creep and strength retention at high temperature was made during alloy design, along with some modification of grain size to optimise this balance, principally adopting sub-solvus heat treatments due to its high γ' solvus temperatures (~1190°C) [1, 25-28]. A great deal of research has illustrated that N18 has good phase stability up to 700^{o}C and possesses high strength and creep resistance associated with a good damage tolerance capability up to 650^{o}C [1, 25]. It is also reported that N18 has better fatigue crack growth resistance compared with fine grained Inconel 718 and Astroloy under the same testing conditions [1]. However, most of these studies have been conducted at 650^{o}C or even lower temperature, where the role of

oxidation may be less significant in assisting fatigue failure processes. To enable a better understanding of the interaction between oxidation and fatigue performance (i.e. fatigue crack initiation and propagation) in this alloy, assessment of the fatigue performance of N18 at temperatures close to its limit-use temperatures are necessary. Therefore, in this study, the fatigue crack initiation and propagation behaviour in N18 alloy has been assessed in air and vacuum across a temperature range of 650°C~725°C to elucidate the role of oxidation in the fatigue failure process.

2. Materials and experimental procedures

2.1 Materials

The N18 alloy used in this study was extracted from a hot isostatically pressed (HIP) and forged, heat treated "pancake" (disc precursor) provided by QinetiQ. Its composition (in wt.%) and heat treatment schedules are presented in Tables 1 and 2 respectively. The microstructures of N18 alloy are shown in Fig.1, and the measured γ grain size and the sizes of primary, secondary and tertiary γ′ are shown in Table 3. In addition, pores were rarely observed during microstructural evaluation and it is believed that this low porosity is due to the HIP process undergone by the alloy. The detailed experimental procedures used for this microstructural evaluation were reported previously in Ref. [18].

Table 1 Composition of N18 alloy (in wt.%)

Cr	Co	Mo	Ti	Al	C	B	Hf	Zr	Ni
11.1	15.4	6.44	4.28	4.28	0.022	0.008	0.50	0.019	Bal.

Table 2 Heat treatment of N18 alloy

Subsolvus heat treatment		Aging heat treatment				
1165°C/4h	→ Air cool →	700°C/24h	→ Air cool →	800°C/4h	→ Air cool	

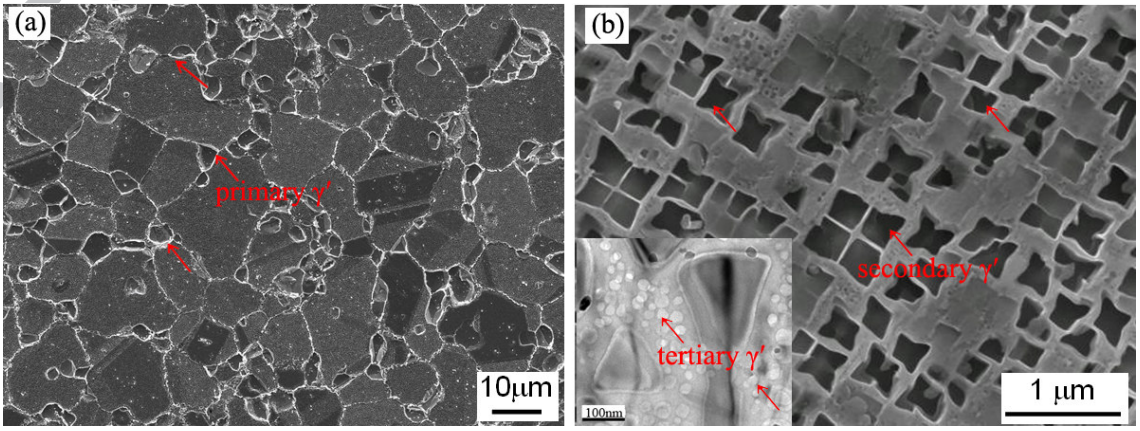

Fig.1 Microstructure of N18 alloy: (a) morphology of grain and primary γ′ and (b) morphology of secondary and tertiary γ′.

Table 3 Grain and γ′ size distributions of N18 alloy

	Grains	Primary γ′	Secondary γ′	Tertiary γ′
Mean size	8.7±4.7 μm	2.19±0.98 μm	188±112nm	25nm

2.2 U-notch fatigue test

Fatigue tests were conducted on polished U-notch specimens under three-point bend loading on an Instron 8501 servo-hydraulic testing machine with an ESH Ltd. high temperature vacuum chamber attached. The test geometry was chosen to assess crack initiation processes and the fatigue performance of N18 in the presence of a stress concentration. As shown in Fig. 2(a), the dimension of the U-notch specimen is 8mm×8mm×50mm, and the radius and the depth of the notch are 2mm and 1.25mm respectively. The notch type was chosen to provide an elastic stress concentration of around 2, i.e. representative of that seen in the fir tree root fixings used to secure blades to turbine discs. The surface of the notch was ground and then was polished using dental felts and 1μm diamond polishing paste. Tests were carried out in air and vacuum (1.0×10^{-3} ~5.0×10^{-2} Pa) at 650 and 725^{o}C under a 1-1-1-1 loading waveform with a load ratio of 0.1. The temperature of the specimen was monitored and controlled to an indicated ±1^{o}C using a Eurotherm 815 thermo-controller and R-type (platinum + 13%rhodium/platinum) thermocouple which was spot welded to the specimen within the hot zone. The span between the two upper rollers is 40mm. The load was applied to produce a maximum nominal elastic stress (σ_{max}) of 1020MPa in the uncracked ligament, defined as the net section bending stress at the plane of the notch root calculated using simple beam theory. The stress distribution across the notch at the maximum and minimum applied loads at 650^{o}C in a quarter of the specimen, calculated in Abaqus by simulating the load roller with an appropriate pressure load and simulating the support roller with a restricted displacement in the vertical direction of the specimen (assuming the contacted region with rollers as elastic to avoid non-convergence in the model), is shown in Fig.2 (c) and (d). The corresponding strains achieved at the notch root are 1.11% and 0.29% respectively according to the finite element simulation. After testing, a JEOL JSM 6500F field emission gun (FEG) scanning electron microscope (SEM) was employed to examine the morphology of fracture surface and the notch root surface.

To further investigate fatigue crack initiation processes, two more interrupted tests were conducted at 650°C in air and vacuum. After each interruption, the specimen was taken out and observed in the SEM, and then the test resumed until apparent cracks appeared at the notch root. Energy dispersive X-ray spectrometry (EDS) was employed to analyse the chemical element distribution around the cracks.

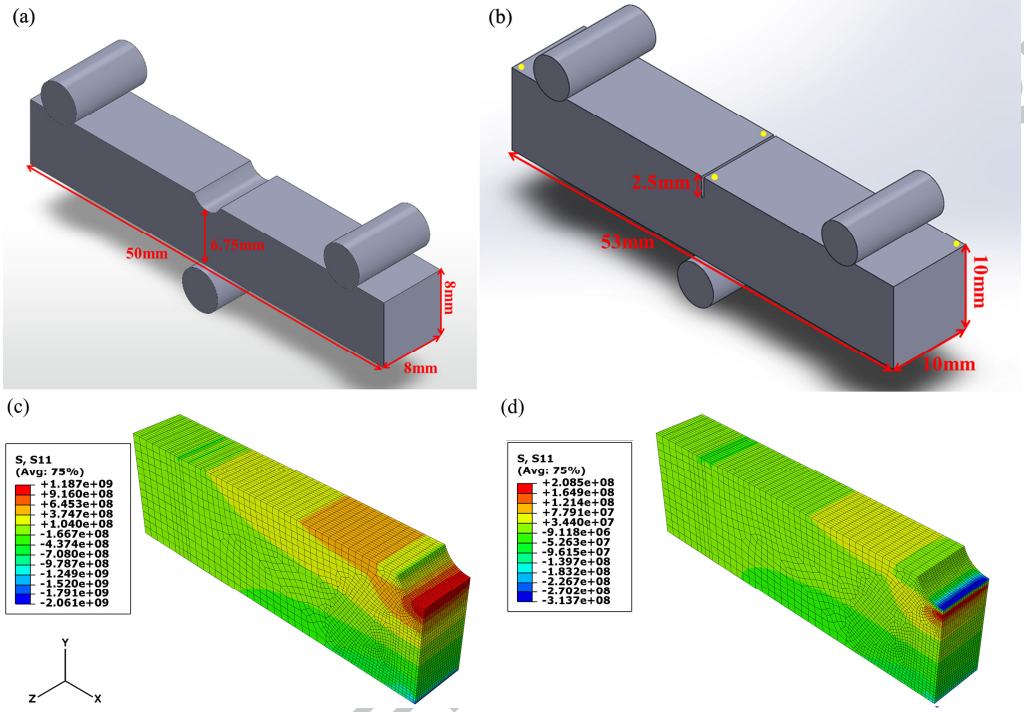

Fig. 2 Schematic diagram of set-up of (a): U-notch fatigue test and (b) long fatigue crack growth test (The small yellow circles on the top surface of the sample shown in (b) indicate the location of electrical potential wires); S_{11} (Pa), stress along the xx direction in a quarter of the U-notch specimen at (c) maximum and (d) minimum load for the 1-1-1-1 loading waveform at 650°C.

2.3 Long fatigue crack growth test

Long fatigue crack growth tests were carried out on single edge notched bend (SENB) specimens with a dimension of 10mm×10mm×53mm as shown in Fig. 2(b). A notch with a depth of 2.5mm and a width of 0.35mm produced by electrical discharge machining (EDM) was introduced into the middle of the SENB specimen to act as a stress concentrator and initiate the crack. The temperature control method and the test procedures are as described for the U-notch fatigue test previously, except that both 1-1-1-1 and 1-20-1-1 trapezoidal loading waveforms were used. Crack length was monitored and recorded by a pulsed-direct current

potential drop method using 4 probe wires, and crack growth rate data was obtained from a precracked sample at a ΔK of ~15MPa√m under constant load, thus allowing fatigue crack growth rate as a function of increasing ΔK to be obtained as the crack grew out. The fracture surfaces were observed in a JEOL JSM 6500 SEM at an accelerating voltage of 15 kV.

3. Results

3.1 Fatigue life of N18 alloy

Lifetimes of the U-notch fatigue tests are presented in Table 4. In general, it shows that both testing in air and increasing the temperatures tend to reduce fatigue life; such that the test carried out in air at 725°C has the lowest life of all the specimens tested.

Table 4: Fatigue life of the U-notch fatigue tests tested at a maximum nominal elastic stress of 1020 MPa

Test conditions	650°C Vacuum	650°C Air	725°C Vacuum	725°C Air
Fatigue life	66006	45148	13778	5145

3.2 Fractography of U-notch fatigue tests

Multiple crack initiation is observed on the fracture surfaces of all the failed specimens under the investigated conditions and more crack initiation sites are observed at 725°C than 650°C either in air or vacuum. The number of crack initiation sites identified on the fracture surfaces at 725°C is approximately 2~3 times of that observed at 650°C [29]. Fig.3 presents the typical crack initiation sites observed on the fracture surfaces in air tests conducted at 650 and 725°C. It is found that cracks mainly initiate from oxidized grain boundaries or γ/γ′ interfaces, and then propagate in a transgranular manner at 650°C. Oxide nodules can be seen at the region close to crack initiation sites, and the oxidized grain boundaries and γ/γ′ interfaces are visible at the polished notch root as shown in Fig.3 (a) and (b). Similar fractography can also be observed at 725°C, although the fracture surfaces were somewhat more contaminated. It appears that the crack initiation regions are more intergranular at 725°C.

As shown in Fig.4 (a), it is observed that a crack initiates from a pore at 650°C in vacuum, which is not seen in the air tests, although similar transgranular crack propagation following crack initiation is seen. For the 725°C vacuum test, it seems that cracks initiate intergranularly as observed in the air tests. The oxidized grain boundaries and γ/γ′ interfaces are also observed in the notch root as shown in Fig.4 (b), which can be seen more clearly in Fig. 5(b).

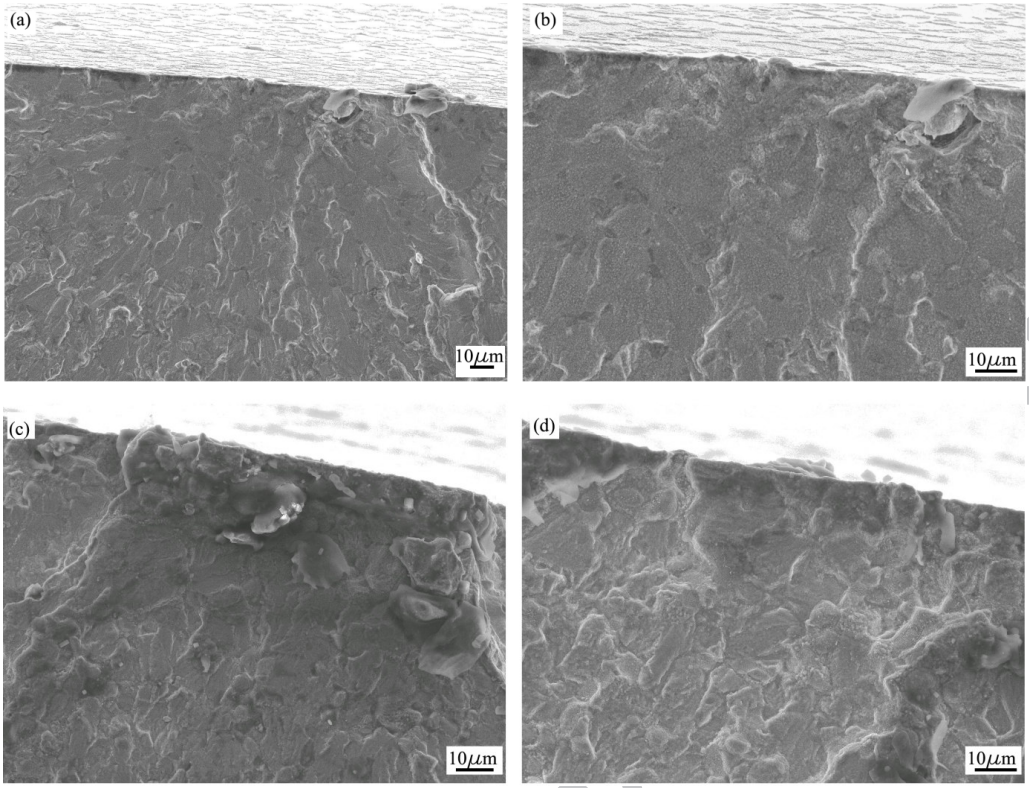

Fig. 3 (a) Fatigue crack initiation sites observed in N18 tested in air at 650°C; (b) higher magnification of crack initiation sites shown in (a);(c) and (d) crack initiation sites at 725°C.

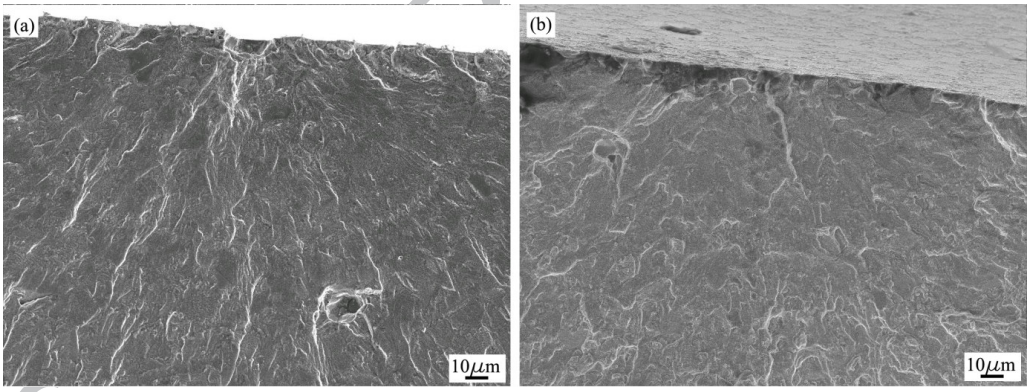

Fig.4 Fatigue crack initiation sites observed in N18 tested in vacuum at (a) 650°C and (b) 725°C.

3.3 Oxidation during U-notch fatigue test

Fig.5 shows the morphology of the notch root of the tested specimens, where oxidation can be clearly seen. As shown in Fig.5 (a) and (b), oxidation occurred at grain boundaries, γ/primary γ′ interfaces and primary γ′ is evident under the vacuum testing conditions, and cracking at these oxidized grain boundaries and γ/γ′ interfaces can be observed. At 725°C, the

γ matrix is also quite severely oxidized, indicated by the oxidized nodules. For the air tests, the oxidation of grain boundaries and γ/γ′ interfaces is even more severe as shown in Fig. 5(c) and (d). It seems that two kinds of oxides with different bulging heights form at the notch root, indicated by different brightness in the SEM secondary electron images. An EDS analysis of these two kinds of oxides indicates that the most significant difference is the Cr enrichment in the dark oxides (Fig. 5(e)) and the Co enrichment in the brighter oxides (Fig.5(f)). It however needs to be pointed out that the quantitative results concerning light elements (i. e. C and O) inserted in Fig. 5 (e) and (f) may be not reliable due to the inherent limitation of the EDS.

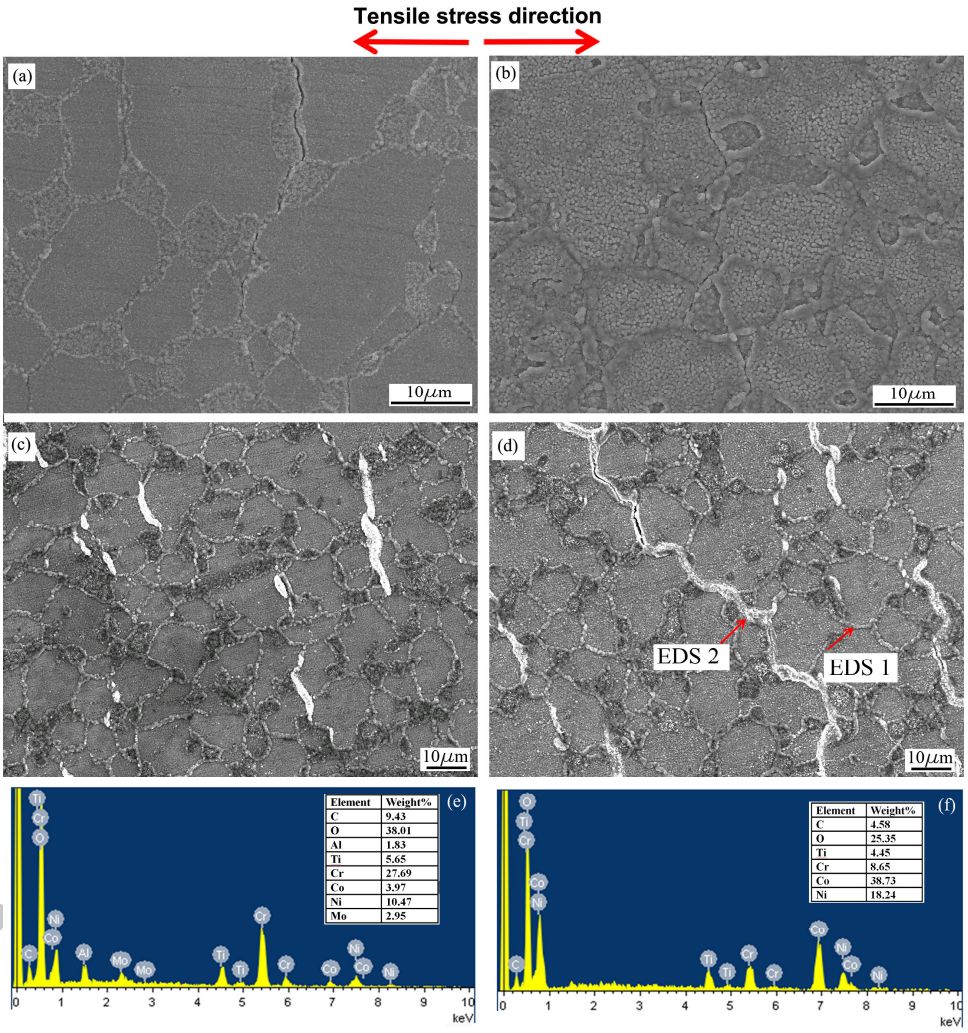

Fig.5 Morphology of notch root after testing: (a) 650°C, vacuum, (b) 725°C, vacuum, (c) 650°C, air and (d) 725°C, air; (e) composition of dark GB oxide detected by EDS 1 and (f)

composition of bright GB oxide detected by EDS 2 shown in (d). The quantitative results corresponding to the EDS spectrums are inserted in (e) and (f) respectively.

The evolution of grain boundary and γ/γ′ interface oxidation and consequent cracking in the interrupted vacuum test is presented in Fig.6. Occasional oxide cracking can be found in the early stages of fatigue life as shown in Fig. 6(a). Multiple grain boundary cracking and/or γ/γ′ interface cracking are clearly observed at the notch root as shown in Fig. 6 (c) and (d).The cracking is more likely to occur at the γ/γ′ interfaces, although GB cracking can also be observed (as shown in Fig.6 (b) ~ (d)). Oxides are observed at some segments along some of the cracked grain boundaries and γ/γ′ interfaces, but most regions of the cracked grain boundaries and γ/γ′ interfaces are not decorated with oxides. An EDS mapping of the cracked region (shown in Fig.6 (d)) is presented in Fig.6 (e), showing an enrichment of Cr and O and a depletion of Ni and Co along the crack path. An enrichment of O can also be observed within the primary γ′ which is enriched in Al and Ti, although this enrichment is not as significant as that along the crack path. A slight enrichment of Al and Ti at grain boundaries can be discerned.

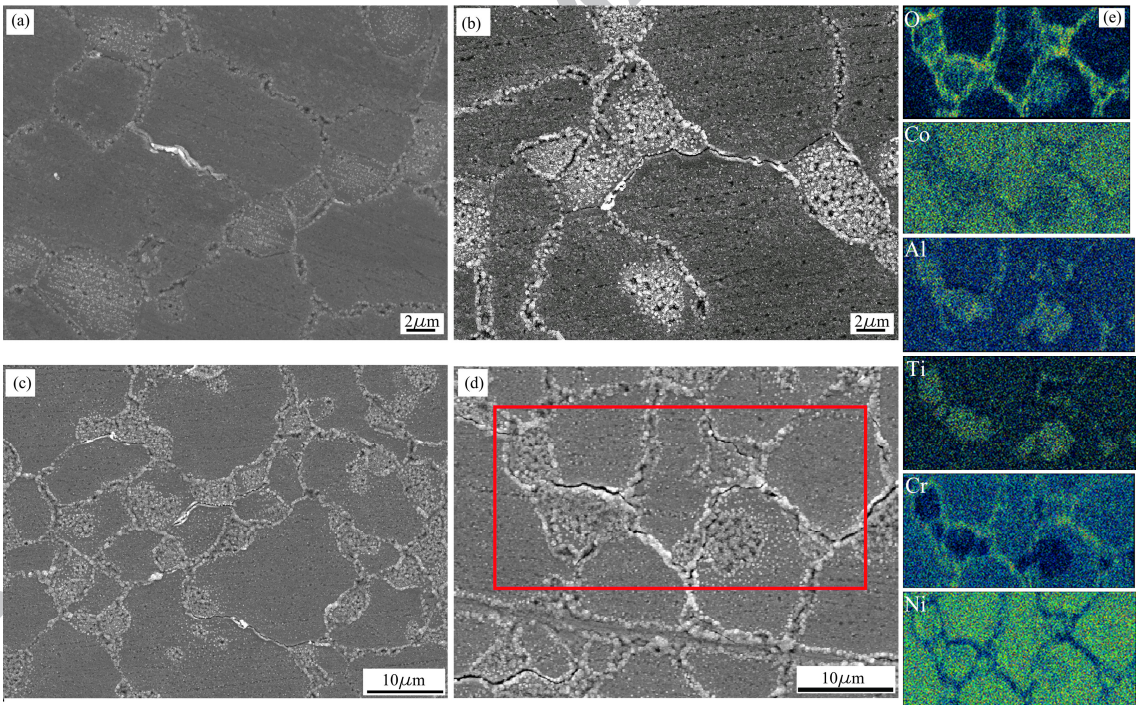

Fig.6 Evolution of cracks from the oxidized grain boundaries and γ/γ′ interfaces at the notch root in the interrupted vacuum test at 650°C: (a) 9000 cycles, (b) 15000 cycles, (c) 31000 cycles and (d) 36000 cycles; (e) EDS mapping of the region highlighted by the rectangle shown in (d).

A similar EDS mapping conducted on the cracked grain boundaries in the interrupted air test, is presented in Fig. 7. As shown, an enrichment of Co and O along with depletion in other elements is found along the grain boundaries decorated with cracked oxides. However, no apparent enrichment of Co and O can be found along the cracked grain boundaries. For other grain boundaries, a slight enrichment of Cr can be seen.

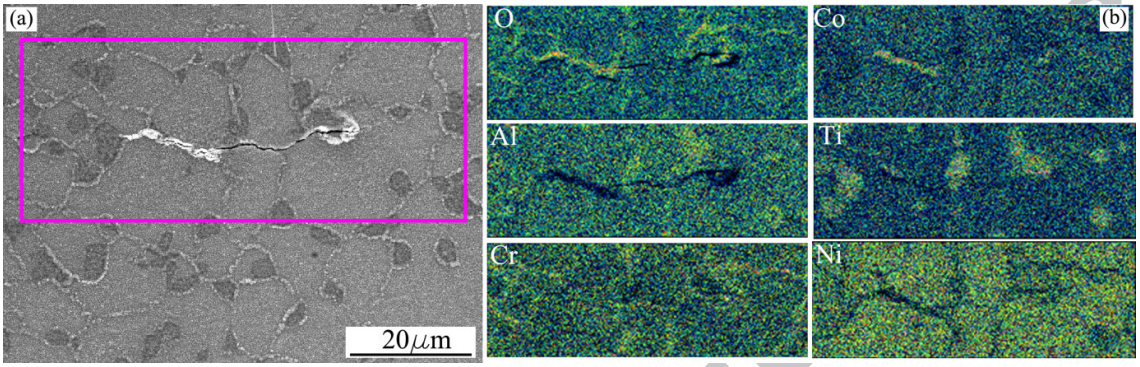

Fig.7 (a) Cracks at the notch root of the interrupted air test at 650°C after 35000 cycles and (b) EDS mapping of the cracked region highlighted by rectangle shown in (a).

3.4 Long fatigue crack growth behaviour

Fig.8 compares the long fatigue crack growth rates of N18 alloy. The data of the tests with a 20s dwell (1-20-1-1) at the peak load was presented to allow a comparison with the data from tests with a 1s dwell (1-1-1-1) [4]. It is found that the oxidizing environment significantly accelerates fatigue crack growth under the investigated conditions. The influence of temperature on fatigue crack growth is dependent on the loading waveform (dwell at maximum load). As shown in Fig.8 (a), only a slight increase in fatigue crack growth rate can be observed either in air or vacuum when temperature is increased from 650°C to 725°C for the 1-1-1-1 tests, whereas the fatigue crack growth rate increases by a factor of 6~7 as temperature increases in the tests with a 20s dwell as shown in Fig.8 (b).

In order to compare the influence of the dwell time on fatigue crack growth rate, a re-plot of Fig.8 is presented in Fig.9, where a significant acceleration in crack growth rate can be seen when a 20s dwell is applied at 725°C either in air or vacuum, but no apparent increase in crack growth rate can be found when the dwell is applied at 650°C.

As shown in Fig.10, the fractography of the air tests at $\Delta K=30MPa\sqrt{m}$, failure becomes increasingly intergranular with the increased temperatures and/or longer dwell period at the peak load. In the 650°C test under 1-1-1-1 waveform, the fracture surface is predominantly transgranular (Fig.10 (a)). When the temperature is increased to 725°C under the 1-1-1-1

waveform or an introduction of 20s dwell at 650°C, the fracture surface is characterized by the mixed-trans-intergranular features (Fig. 10 (b) and (c)). In the 725°C test with a 20s dwell, the fracture surface is mainly intergranular and oxide nodules can be clearly seen on the fracture surface (Fig. 10 (d)).

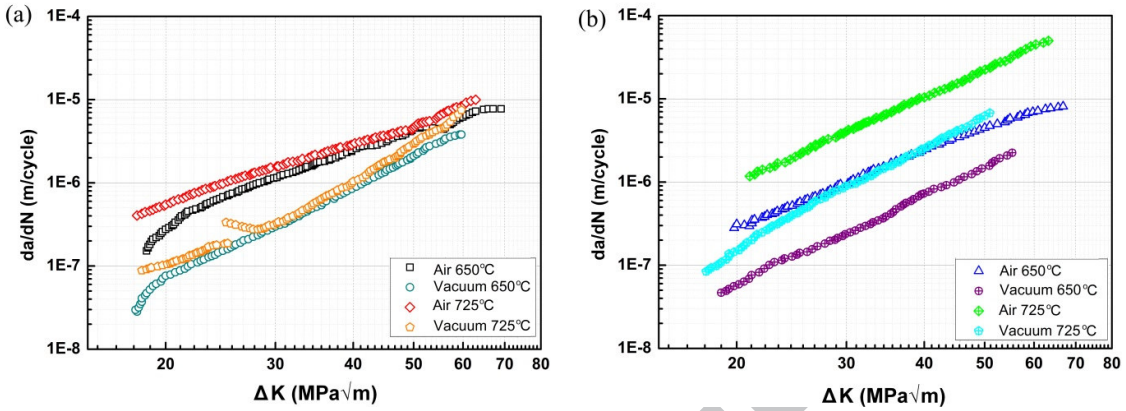

Fig.8 Effect of environment and temperature on fatigue crack growth under (a) 1-1-1-1 and (b) 1-20-1-1 loading waveforms.

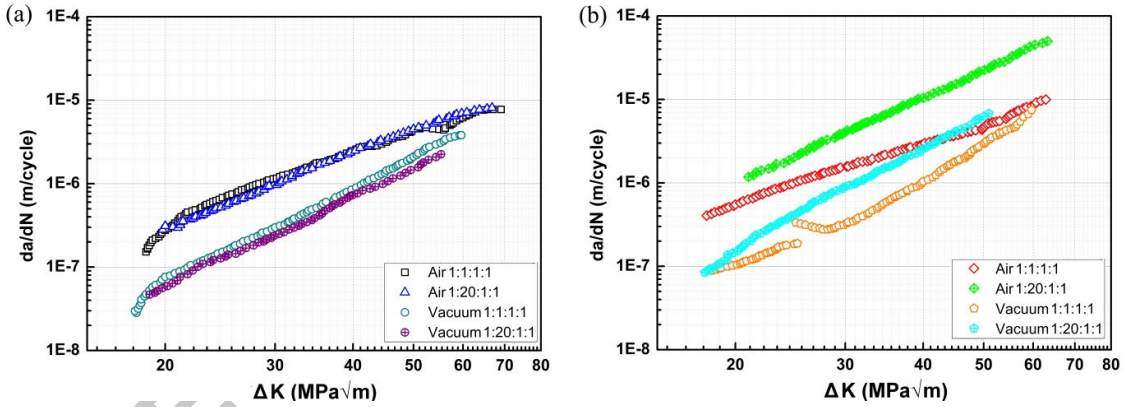

Fig.9 Effect of environment and dwell time at the peak load on fatigue crack growth at (a) 650°C and (b) 725°C.

Fig.11 presents the fractography of the vacuum tests at ΔK=30MPa√m. As temperature increases or with the introduction of a longer dwell time at the peak load, a similar variation in intergranular/transgranular fracture surface features can be found as observed in the air tests, although the fracture surfaces are more transgranular generally. As shown in Fig.11 (a) and (b), the fracture surfaces of the tests under 1-1-1-1 waveform are predominantly transgranular, even though slightly more intergranular features can be discerned at 725°C. Apparent nodules can be found on the fracture surfaces in the tests with a 20s dwell either at

650°C or 725°C. For the 725°C test with a 20s dwell, the fracture surface is predominantly intergranular as shown in Fig. 11 (d).

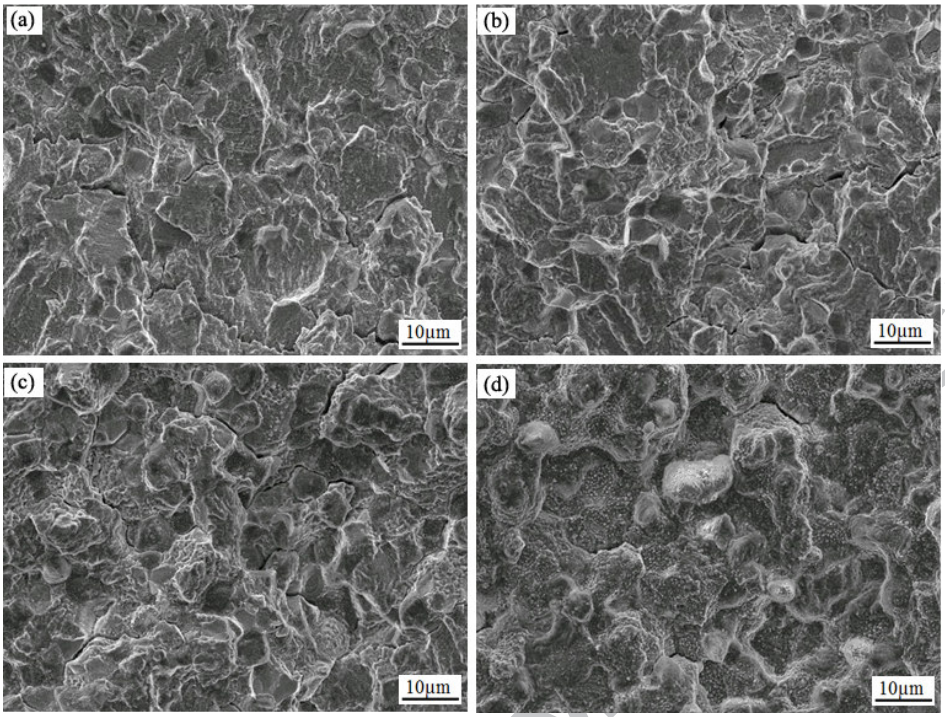

Fig.10 Fractography of air tests at a ΔK=30MPa√m: (a) 650°C, 1-1-1-1 waveform, (b) 725°C, 1-1-1-1 waveform, (c) 650°C, 1-20-1-1 waveform and (d) 725°C, 1-20-1-1 waveform.

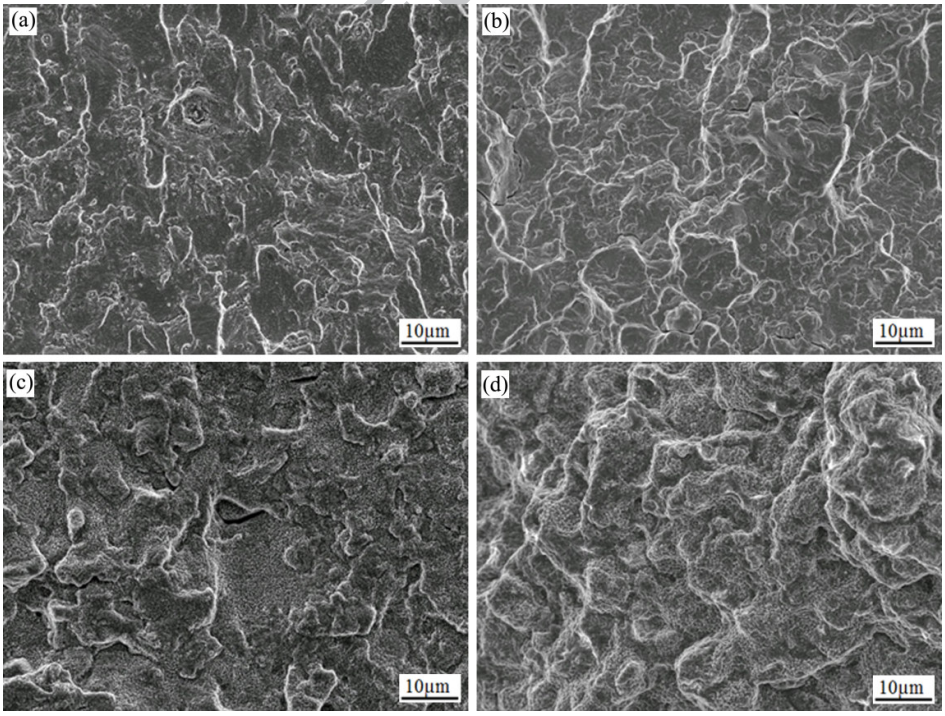

Fig.11 Fractography of vacuum tests at a ΔK=30MPa√m: (a) 650°C, 1-1-1-1 waveform, (b) 725°C, 1-1-1-1 waveform, (c) 650°C, 1-20-1-1 waveform and (d) 725°C, 1-20-1-1 waveform.

4. Discussion

4.1 Effect of oxidation on fatigue life

It is can be seen in this study that there is a strong dependence of the fatigue performance on the oxidation processes that have occurred in N18. The reduction in fatigue life in oxidizing environment or at higher temperatures (shown in Table 4) is apparently linked to the formation of Co-rich and/or Cr-rich oxide at grain boundaries and γ/γ′ interfaces and subsequent oxide cracking. By comparing fatigue lives of the U-notch specimens and long crack growth rates obtained in the tests under a 1-1-1-1 loading waveform, it can be seen that the temperature effect is quite minimal on fatigue crack growth rates in either vacuum or air, and it can be seen that it is the effect of an oxidation environment that significantly accelerates crack growth rates, rather than temperature alone. The U-notch fatigue life (under a 1-1-1-1 waveform) is also significantly reduced at both 650°C and 725°C in air compared to in vacuum, but the lifetime in air or vacuum is also noticeably lower at 725°C *cf* 650°C. These differences in oxidation effects with temperature indicate that the fatigue life of the U-notch N18 specimens under the investigated conditions is not simply due to crack propagation differences but may be more determined by the crack initiation process, but perhaps also the expected strain ranges achieved in the notch root at the same nominal stress level. In order to further assess the possible effects of crack initiation and propagation processes on fatigue life under this loading waveform of 1-1-1-1, a simple crack propagation life assessment has been considered for the different test conditions. Numerical iterations of crack growth based on the differing long crack Paris laws for the different conditions have been compared for a single assumed initial crack of 10μm (which is approximately equivalent to a grain size, thus assuming intergranular crack initiation). The details of the numerical iteration are shown in the Appendix, and the calculated crack propagation life to reach a nominal ΔK of 52 MPa√m is shown in Table 5 and compared to the total observed life and the apparent initiation life. This ranking of nominal propagation life allows a better quantification of the simple effect of crack growth rate on lifetimes.

By making a comparison with the measured total fatigue life, it is found that the nominal crack initiation life could account for a major part of the fatigue life either in air or in vacuum, indicating the cycles to produce crack initiation contribute more to the total observed life. As shown in Table 5, more cycles are required for crack initiation at 650°C than 725°C either in

air or vacuum, this may be because the oxides are expected to form and subsequently crack after shorter times at 725°C due to the higher expected diffusivity of oxygen and oxide-forming elements [21, 30]. Similarly, more cycles are required for crack initiation in vacuum than in air either at 650°C or 725°C, but this difference is much less significant compared with the difference of crack initiation cycle between 650°C and 725°C, which indicates that the temperature (rather than availability of oxygen) is the rate-determining factor for oxidation during the crack initiation stage in this study in light of the relatively low vacuum used. Although it is expected that it may take more cycles for crack initiation at lower oxygen partial pressure, the apparent contribution of crack initiation to fatigue life is less significant in vacuum than that in air (65% vs. 93.2% at 650°C and 52.7% vs. 73.3% at 725°C respectively), which may be associated with the slower crack propagation in vacuum due to the less severe oxidation ahead of crack tip.

Table 5 Comparison of nominal fatigue crack propagation life, N_g, initiation life, N_i, and total life, N_{tot}

Test conditions	650°C Vacuum	650°C Air	725°C Vacuum	725°C Air
Nominal crack propagation life, N_g	23087	2858	6511	1376
Nominal crack initiation life, N_i	42919	42290	7267	3769
Total life, N_{tot}	66006	45148	13778	5145
N_i/N_{tot} (%)	65	93.2	52.7	73.3

Of course in such an approach several assumptions are made that do not reflect the real physics of the situation: long crack growth behaviour will not represent the crack growth behaviour for such small cracks in the elasto-plastic notch stress field (in fact previous work in IN718 notch fatigue samples has indicated a constant crack growth rate may occur under such conditions [19]); this approach also only considers the growth of a single crack and ignores any coalescence effects. Coalescence events are evident in these fatigue tests due to the multiplicity of crack initiation events and may play a more critical role in controlling the crack propagation lifetime and thereby the overall lifetime. The effect of the positioning of neighbouring cracks on the propagation of individual short cracks and subsequent coalescence events has not been considered in detail in this simple lifing assessment. This approach does however allow for an element of quantification of the likely contribution of differences in crack growth rates in explaining the observed lifetimes. The short crack growth behaviour has not been quantified (due to the difficulties in conducting a replica analysis with associated, pump-down, reheating and cooling cycles which may in themselves significantly

affect short crack growth behaviour), but our study on fine grained LSHR alloy (which has a similar microstructure to N18) with interrupted fatigue tests along with a replication procedure shows that the initiation of GB cracks accounts for the majority of the fatigue life, and fracture occurs within a short period by a rapid coalescence of these GB cracks [31]. Similar effects of oxidation on fatigue life have also been observed in other disc alloys such as ME3 [10]. Low cycle fatigue tests conducted on ME3 that was pre-exposed at different elevated temperatures for varying periods showed that the reduction in fatigue life is determined by the net oxidation effect, i.e. depth of oxide layer and the oxidation affected zone (which is used to refer to the GB carbide dissolution region), rather than simply by temperature or exposure time. By removing the oxide layer and oxidation affected zone in the pre-exposed ME3, the fatigue life was significantly improved, to become close to the fatigue life of un-exposed specimens, due to the suppression of intergranular crack initiation and the reduction in crack initiation sites, although the same intergranular crack propagation immediately sets in after transgranular crack initiation, indicating the predominant contribution of the crack initiation process to fatigue life [10].

Previous work in other systems (e.g. in austempered ductile irons at room temperature) has shown that short crack growth behaviour can be dramatically different where significant micro-crack fields are formed. Where initiation processes were very easy (e.g. cracking of multiple carbides [32]]) subsequent crack growth was observed to be extremely slow, as the closely neighbouring cracks robbed surrounding crack tips of the required strain fields to propagate and lifetime was effectively controlled by coalescence events. In some cases a microcracking field can occur ahead of the crack tip, contributing significantly to crack propagation resistance [33]. Hence, to fully understand the relative contributions of crack initiation processes and subsequent growth to overall lifetime requires a probabilistic assessment of coalescence behaviour rather than just simple Paris lifing approaches.

4.2 Role of oxidation in crack initiation

Unlike at room temperature where cracks mainly initiate from slip bands at low strain levels and may initiate from GB boundaries at high strain levels, cracks mainly initiate from grain boundaries under these investigated conditions (along with occasional pore-initiation in vacuum at 650^{o}C). Intergranular crack initiation can be seen more clearly from the notch root observations in the interrupted tests. With increased temperature (associated with enhanced oxidation effects), pore-initiation is suppressed. Intergranular crack initiation at elevated

temperatures usually results from GB oxide cracking or the embrittlement effect due to the absorption of oxygen and other embrittling elements leading to the decrease in cohesion strength of grain boundaries [10, 16, 19, 20]. In this study, it appears that GB oxide cracking makes the main contribution to crack initiation as shown clearly in Figs. 6 and 7. With the formation and build-up of GB oxides, stress will develop within the oxide due to volume expansion caused by the difference in density between Cr-rich or Co-rich oxides and the matrix. Additionally, the notch root stress concentration will introduce additional stress to the oxides [34]. Furthermore, these GB oxides can act as stress concentration sites during fatigue loading, and thereby more easily fracture and result in crack initiation. The reason some grain boundaries oxidise and form cracks preferentially needs further elucidation, but may be due to differences in plastic strain accumulation and hence stress assisted oxidation processes.

4.3 Role of oxidation in crack growth

Crack growth in disc alloys at elevated temperatures under cyclic load usually arises from damage via fatigue, creep and oxidation processes, as well as their combined effects [4, 6, 10, 17, 18, 30]. As shown in Figs. 8 and 9, the crack growth rate is higher in air than in vacuum when other test conditions are identical, indicating the significant influence of oxygen partial pressure. The effect of oxidation (brought by the variation of oxygen partial pressure) on crack growth can be further verified by the mixed inter-transgranular features on fracture surface in air *cf.* completely transgranular features on the fracture surface in vacuum under the 1-1-1-1 loading waveform, as shown in Figs. 10 and 11. This observation is consistent with Molins' study [6] and is believed to be associated with the oxidation process ahead of the crack tip. Although no direct observation of the crack tip has been made in this study, a recent study on oxidation ahead of a crack tip in RR1000 shows that layered oxides (which consist of a thermodynamically unstable central layer of NiO/CoO and a thermodynamically stable marginal layer of Cr/Al/Ti oxides) form ahead of the crack tip [13]. This suggests that the dense oxides such as Cr_2O_3 and Al_2O_3 form under the low oxygen partial pressure, whereas the less dense or porous oxides such as NiO and CoO form under the relatively high oxygen partial pressure. The oxide intrusion ahead of the crack tip formed under dynamic load is much shorter than that formed under static load, indicating that the crack grows by oxide cracking/spallation [13]. Unlike environment/oxygen partial pressure, the influences of dwell time and temperature on crack growth rate appear to depend on each other, i.e. the apparent accelerated effect of dwell time on crack growth rate can only be observed at 725^{o}C. The effect on crack growth brought about by increased dwell period or temperature can be

linked to oxidation as well as creep [18, 35], but it is difficult to quantitatively separate or identify the contribution of oxidation and creep to crack growth respectively as these two processes may occur simultaneously, even in the nominal "vacuum" conditions in this study.

In order to further assess the contribution of creep and/or oxidation processes to crack growth, an apparent activation energy analysis has been carried out (as creep and oxidation are thermally activated processes). The details of this analysis method can be found in Ref. [35]. In brief it assumes that the rate of the thermally activated process is proportional to an Arrhenius term, and the apparent activation energy of crack growth can be obtained from two fatigue crack propagation tests, carried out at T_2 and T_1:

$$Q = \frac{-R_g}{T_2^{-1} - T_1^{-1}} \ln \left(\frac{da}{dN}(T_2) \Big/ \frac{da}{dN}(T_1) \right)$$

Where Q is the apparent activation energy, and R_g is the gas constant (8.31 J/mol K).

The calculated apparent activation energies for crack growth in N18 under the investigated conditions are shown in Fig. 12, and the activation energies of the related thermally activated processes reported in the literature are shown in Table 6 [8, 35, 36]. It seems that any additional oxidation brought about by increased dwell time and/or temperature makes little contribution to crack growth rates under the investigated conditions, this differs from our findings for LSHR alloy, a more creep-resistant but more oxidation-sensitive disc alloy [4]. For N18, it appears that the GB creep process is promoting crack growth when a dwell of 20s at the peak load is introduced during the tests, indicated by the calculated activation energy which is quite close to the reported activation energy of GB creep processes. For the tests conducted under a 1-1-1-1 loading waveform, the obtained apparent activation energy is much lower than that of GB creep processes, indicating limited creep is activated. In this case, the slight increase in crack growth rate with temperature may arise from the very slight decrease in yield strength with the increasing temperature (i.e. $\sigma_{0.2\%}$ 1031MPa at 650°C, and 1016MPa at 725°C [29]). As mentioned previously, the effect of oxidation has been discerned by the increasing intergranular features observed on the fracture surfaces when changing the test environment from vacuum to air, but this may not have significantly affected the crack growth rate (on the basis of the apparent activation energy analysis comparison). Furthermore, it should be noted that increased intergranular features on the fracture surfaces when introducing a 20s dwell may also indicate the activation of creep processes, and this change in fracture surface feature is most significant at 725°C in vacuum (where oxidation may be expected to be suppressed).

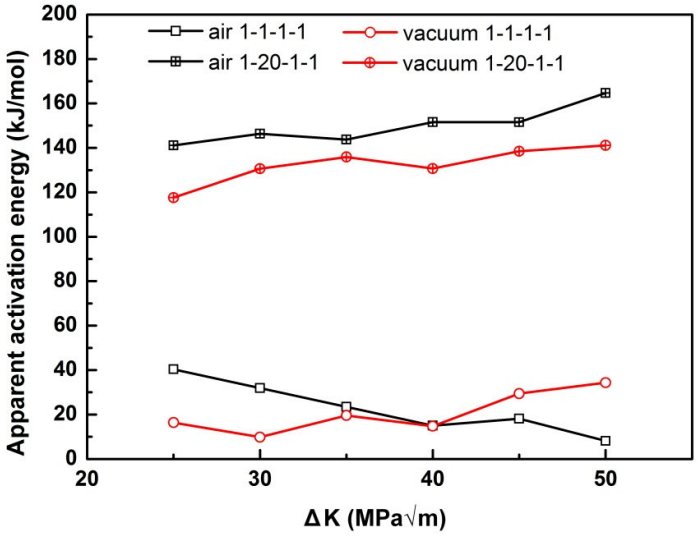

Fig.12 Apparent activation energies for fatigue crack growth in N18 tested at 650 and 725°C in air and vacuum under a 1-20-1-1/1-1-1-1 loading waveform.

Table 6 Activation energies for processes contributing to high temperature fatigue crack growth [8, 35, 36]

Processes contributing to high temperature fatigue crack growth	Activation energy (kJ/mol)
Oxidation of Carbides	~ 250
Dynamic embrittlement	~ 250
Grain boundary creep	~ 150
Change in static properties	~ 0-60
Grain boundary creep failure + non-thermally activated failure	~ 0-150

5. Conclusion

The fatigue performance of N18 has been assessed at 2 temperatures in air and vacuum under 1-1-1-1 and/or 1-20-1-1 trapezoidal loading waveforms, to elucidate the influence of oxidation along with (possible) creep processes on crack initiation and propagation behaviour. The following conclusions can be made based on the aforementioned results:

(1) Oxidation occurs even though the oxygen partial pressure is as low as 10^{-2}~10^{-3}Pa. Cr-rich oxide forms uniformly along the grain boundaries and at the γ/γ′ interface at the notch surface in both air and vacuum. A selective formation of Co-rich oxide is observed on some grain boundaries and γ/γ′ interfaces.

(2) Cracks mainly initiate from grain boundaries and γ/γ′ interfaces due to oxide cracking at these regions in both air and vacuum, and occasionally initiate from surface/subsurface pores in vacuum. The crack initiation process and subsequent coalescence events appear to have a significant effect on the fatigue life of notched N18 samples. With an increased test temperature and/or application of an oxidizing environment, fatigue life is reduced markedly, which is associated with the accelerated oxide formation and crack initiation processes, although nominal crack propagation lives also decrease.

(3) Oxygen partial pressure (test environment) has a significant influence on crack growth. Much higher crack growth rates associated with more intergranular fracture surfaces are observed in air compared with in vacuum under the same loading and temperature conditions. An apparent activation energy analysis approach reveals that additional oxidation effects brought about by increasing temperature or prolonging the dwell period on crack growth appear limited. The prolonged dwell period instead apparently promotes creep processes, which further enhance crack growth, especially at higher temperature.

6. Acknowledgements

The authors would like to express their gratitude to University of Southampton, UK, the China Scholarship Council, China, the Engineering and Physical Science Research Council (EPSRC), UK and QinetiQ Ltd., Farnborough, UK for financial support. SNECMA is thanked for supply of N18. The authors also would like to thank Miss Binyan He at University of Southampton for the helpful discussion about ΔK calibration for the numerical integration of the Paris laws.

7. Appendix

This appendix provides details of the Numerical integration of the Paris equations. An assumption of long crack growth behaviour is made after intergranular crack initiation. The Paris equation is shown as follows:

$$\frac{da}{dN} = C\Delta K^m \quad \text{(A1)}$$

where C and m are materials-specific constants, and they are derived from the crack growth rate between ΔK of 20~50MPa√m shown in Fig.8(a). For 725°C vacuum test, two fitting

processes were conducted to get the *C* and *m* values as there is an interruption in the fatigue crack growth curve. The obtained *C* and *m* values are shown in Table A1.

Table A1 Fitted *C* and *m* values for the Paris equation for fatigue crack growth under a 1-1-1-1 loading waveform

Tests	650°C Vacuum	650°C Air	725°C Vacuum	725°C Vacuum	725°C Air
ΔK range	20~50	20~50	20~25	26~50	20~50
C	1E-12	1E-10	4E-11	4E-13	7E-10
m	3.645	2.665	2.649	4.051	2.249

ΔK calculation is based on the empirical formula developed by Scott and Thorpe [37]

$$\Delta K = B_w \cdot M_{f(\frac{\pi}{2})}\left[1 - 1.36\left(\frac{a}{w}\right)\left(\frac{a}{c}\right)^{0.1}\right]\frac{1}{E(K)}\Delta\sigma\sqrt{\pi a} \quad \text{(A2)}$$

where $\Delta\sigma$ is stress range applied to notch root, which is calculated to be 1500MPa at 650°C as shown in Fig. 2(c) and (d). The stress and strain distribution at 725°C is quite similar to that at 650°C based on the finite element modelling for the employed test conditions as the yield strengths of N18 at 650 and 725°C are quite close to each other [29]. Thus, $\Delta\sigma$=1500Mpa is also used for ΔK calculation at 725°C. *a* is crack depth at the notch root, *c* is half crack length at notch root surface, *w* is sample thickness. In this study, all K calculations assume a crack depth to half surface crack length ratio (*a/c*) of 1. B_w is a correction factor for the finite dimension of the investigated samples, and it is dependent on crack and sample dimensions [38].

$$B_w = 1 + \frac{F(\frac{a}{c})G(\frac{c}{b})H(\frac{a}{w})}{(0.2745)^2} \quad \text{(A3)}$$

where

$$F\left(\frac{a}{c}\right) = 0.38 - 0.141\left(\frac{a}{c}\right) - 0.366\left(\frac{a}{c}\right)^2 + 0.569\left(\frac{a}{c}\right)^3 - 0.248(\frac{a}{c})^4 \quad \text{(A4)}$$

$$G\left(\frac{c}{b}\right) = -0.0239 + 1.434\left(\frac{c}{b}\right) - 2.984\left(\frac{c}{b}\right)^2 + 7.822(\frac{c}{b})^3 \quad \text{(A5)}$$

$$H\left(\frac{a}{w}\right) = -0.0113 + 0.323\left(\frac{a}{w}\right) + 0.749\left(\frac{a}{w}\right)^2 - 0.535(\frac{a}{w})^3 \quad \text{(A6)}$$

where *b* is the width of samples.

$M_{f(\frac{\pi}{2})}$ is front face correction factor for crack shape and *E(K)* is the elliptic integral of the second kind.

$$M_{f(\frac{\pi}{2})} = 1.13 - 0.07\left(\frac{a}{c}\right)^{0.5} \quad \text{(A7)}$$

$$E(K) = [1 + 1.47\left(\frac{a}{c}\right)^{1.64}]^{0.5} \quad \text{(A8)}$$

If

$$Y = B_w M_{f(\frac{\pi}{2})}[1 - 1.36\left(\frac{a}{w}\right)\left(\frac{a}{c}\right)^{0.1}]\frac{1}{E(K)} \quad \text{(A9)}$$

Then

$$\frac{da}{dN} = c[Y\Delta\sigma\sqrt{\pi a}]^m \quad \text{(A10)}$$

$$\int_0^{N_f} dN = \frac{1}{C(\Delta\sigma)^m}\int_{a_i}^{a_f}\frac{da}{(Y\sqrt{\pi a})^m} \quad \text{(A11)}$$

For a small enough crack increment (Δa) of 10 μm, Y_j can be considered as constant. Thus for a crack growth from length a_j to $a_j + \Delta a$,

$$\Delta N_j = \frac{1}{C(\Delta\sigma)^m}\int_{a_j}^{a_j+\Delta a}\frac{da}{(Y_j\sqrt{\pi a})^m} = \frac{1}{C(\Delta\sigma)^m}\frac{1}{(Y_j\sqrt{\pi})^m}\left(\frac{2}{2-m}\right)\left[\left(a_j + \Delta a\right)^{1-\frac{m}{2}} - {a_j}^{1-\frac{m}{2}}\right] \quad \text{(A12)}$$

Hence,

$$N_f = \sum_{j=1}^{j=n}\Delta N_j = \frac{2}{2-m}\frac{1}{C(\Delta\sigma\sqrt{\pi})^m}\sum_{j=1}^{j=n}\frac{(a_j+\Delta a)^{1-\frac{m}{2}} - {a_j}^{1-\frac{m}{2}}}{(Y_j)^m} \quad \text{(A13)}$$

where *n*=220, corresponding to a final crack length of 2.2mm in depth direction at notch root (which is consistent with main crack propagation depth on fracture surface) and a ΔK of ~52MPa√m.

8. Reference

[1] J. Guedou, J. Lautridou, Y. Honnorat, Journal of Materials Engineering and Performance, 2 (1993) 551-556.
[2] R.C. Reed, Cambridge University Press, (2006).
[3] D. Furrer, H. Fecht, Journal of the Minerals, Metals and Materials Society, 51 (1999) 14-17.
[4] S. Everitt, R. Jiang, N. Gao, M. J. Starink, J. W. Brooks and P. A. S. Reed, Materials Science and Technology, 29 (2013) 781~787.
[5] H.T. Pang, P.A.S. Reed, Materials Science and Engineering: A, 448 (2007) 67-79.
[6] R. Molins, G. Hochstetter, J.C. Chassaigne, E. Andrieu, Acta Materialia, 45 (1997) 663-674.
[7] J. Tong, J. Byrne, Fatigue & Fracture of Engineering Materials & Structures, 22 (1999) 185-193.
[8] L. Ma, K.-M. Chang, Scripta Materialia, 48 (2003) 1271-1276.
[9] T.P. Gabb, J. Gayda, J. Telesman, L.J. Ghosn, A. Garg, International Journal of Fatigue, 48 (2013) 55-67.

[10] C.K. Sudbrack, S.L. Draper, T.T. Gorman, J. Telesman, T.P. Gabb, D.R. Hull, Oxidation and the Effects of High Temperature Exposures on Notched Fatigue Life of an Advanced Powder Metallurgy Disk Superalloy, in: Superalloys 2012, John Wiley & Sons, Inc., 2012, pp. 863-872.
[11] E. Andrieu, R. Molins, H. Ghonem, A. Pineau, Materials Science and Engineering: A, 154 (1992) 21-28.
[12] C.F. Miller, G.W. Simmons, R.P. Wei, Scripta Materialia, 48 (2003) 103-108.
[13] H.S. Kitaguchi, H.Y. Li, H.E. Evans, R.G. Ding, I.P. Jones, G. Baxter, P. Bowen, Acta Materialia, 61 (2013) 1968-1981.
[14] J.A. Pfaendtner, C.J. McMahon Jr, Acta Materialia, 49 (2001) 3369-3377.
[15] U. Krupp, W.M. Kane, C. Laird, C.J. McMahon, Materials Science and Engineering: A, 387–389 (2004) 409-413.
[16] A. Pineau, S.D. Antolovich, Engineering Failure Analysis, 16 (2009) 2668-2697.
[17] P.A.S. Reed, Materials Science and Technology, 25 (2009) 258-270.
[18] R. Jiang, S. Everitt, M. Lewandowski, N. Gao; P. A. S. Reed, International Journal of Fatigue, 62 (2013) 217-227.
[19] T. Connolley, P.A.S. Reed, M.J. Starink, Materials Science and Engineering: A, 340 (2003) 139-154.
[20] D.A. Woodford, Energy Materials: Materials Science and Engineering for Energy Systems, 1 (2006) 59-79.
[21] A. Karabela, L.G. Zhao, J. Tong, N.J. Simms, J.R. Nicholls, M.C. Hardy, Materials Science and Engineering: A, 528 (2011) 6194-6202.
[22] J. Gayda, R.V. Miner, International Journal of Fatigue, 5 (1983) 135-143.
[23] J. Gayda, R. Miner, Metallurgical and Materials Transactions A, 14 (1983) 2301-2308.
[24] S. Everitt, M. J. Starink, H. T. Pang, I. M. Wilcock, M. B. Henderson and P. A. S. Reed, Materials Science and Technology, 23 (2007) 1419-1423.
[25] E. Andrieu, A. Pineau, Journal De Physique Iv, 9 (1999) 3-11.
[26] F. Sansoz, B. Brethes, A. Pineau, Fatigue & Fracture of Engineering Materials & Structures, 25 (2002) 41-53.
[27] B. Flageolet, M. Jouiad, P. Villechaise, J. Mendez, Materials Science and Engineering: A, 399 (2005) 199-205.
[28] J.A. Ruiz-Sabariego, S. Pommier, International Journal of Fatigue, 31 (2009) 1724-1732.
[29] S. Everitt, PhD Dissertation, Developments in advanced high temperature disc and blade materials for aero-engine gas turbine applications, University of Southampton, (2012).
[30] L.G. Zhao, J. Tong, M.C. Hardy, Engineering Fracture Mechanics, 77 (2010) 925-938.
[31] R. Jiang, N. Gao, P. A.S. Reed, Depenence of small crack initiation and proapgation on grain orientation in LSHR alloy at elevated temperatures, Under preparation, (2014).
[32] B. Stokes, N. Gao, P.A.S. Reed, K.K. Lee, Metallurgical and Materials Transactions A, 36 (2005) 977-988.
[33] B. Stokes, N. Gao, P.A.S. Reed, Materials Science and Engineering: A, 445–446 (2007) 374-385.
[34] H.E. Evans, International Materials Reviews, 40 (1995) 1-40.
[35] M.J. Starink, P.A.S. Reed, Materials Science and Engineering: A, 491 (2008) 279-289.
[36] M.O. Alniak, F. Bedir, Materials Science and Engineering: A, 429 (2006) 295-303.
[37] P.M. Scott, T.W. Thorpe, Fatigue & Fracture of Engineering Materials & Structures, 4 (1981) 291-309.
[38] S.J. Holdbrook, W.D. Dover, Engineering Fracture Mechanics, 12 (1979) 347-364.

1. Crack initiation is related to Cr and Co oxide formation and cracking in N18
2. Fatigue life appears to be dominated by oxidation-induced crack initiation process
3. Oxidation accelerates crack growth associated with intergranular fracture
4. Long dwell loading cycle causes a superimposed creep damage